

Enhanced transmission through subwavelength apertures by excitation of particle localized plasmons and nanojets

F.J. Valdivia-Valero¹ and M. Nieto-Vesperinas^{1,*}

¹*Instituto de Ciencia de Materiales de Madrid, C.S.I.C., Campus de Cantoblanco
28049 Madrid, Spain*

**mnieto@icmm.csic.es*

Abstract: We study, and illustrate with numerical calculations, transmission enhancement by subwavelength 2D slits due to the dominant role played by the excitation of the eigenmodes of *plasmonic* cylinders when they are placed at the aperture entrance; and also due to reinforced and highly localized energy in the slit as a consequence of the formation of a *nanojet*. We show that, providing the illumination is chosen such that an aperture transmitting eigenmode is generated, the phenomenon is independent of whether or not the slit alone produces extraordinary transmission; although in the former case this enhancement will add to this slit supertransmission. We address several particle sizes, and emphasize the universality of this phenomenon with different materials.

© 2018 Optical Society of America

OCIS codes: (050.1940) Diffraction; (050.1220) Apertures; (050.6624) Subwavelength structures; (160.4236) Nanomaterials; (230.5750) Resonators; (230.7370) Waveguides; (240.6680) Surface plasmons; (250.6715) Switching.

References and links

1. F. J. Garcia de Abajo, “Colloquium: Light scattering by particle and hole arrays”, *Rev. Mod. Phys.* **79**, 1267 – 1290 (2007).
2. F. J. Garcia-Vidal, L. Martin-Moreno, T. W. Ebbesen, L. Kuipers, “Light passing through subwavelength apertures”, *Rev. Mod. Phys.* **82** 729 (2010).
3. T. W. Ebbesen, H. J. Lezec, H. F. Ghaemi, T. Thio, P. A. Wolff, “Extraordinary optical transmission through sub-wavelength hole arrays”, *Nature (London)* **391**, 667 - 669 (1998).
4. H. A. Bethe, “Theory of diffraction by small holes”, *Phys. Rev.* **66**, 163 – 182 (1944).
5. L. Martin-Moreno, F. J. Garcia-Vidal, H. J. Lezec, K. M. Pellerin, T. Thio, J. B. Pendry, and T. W. Ebbesen, “Theory of extraordinary optical transmission through subwavelength hole arrays”, *Phys. Rev. Lett.* **86**, 1114 – 1117 (2001).
6. H. J. Lezec, A. Degiron, E. Devaux, R. A. Linke, L. Martin-Moreno, F. J. Garcia-Vidal, T. W. Ebbesen, “Beaming light from a subwavelength aperture”, *Science* **297**, 820 – 822 (2002).
7. F. J. Garcia de Abajo, “Light transmission through a single cylindrical hole in a metallic film”, *Opt. Express* **10**, 1475 – 1484 (2002).
8. W. L. Barnes, W. A. Murray, J. Dintinger, E. Devaux, and T.W. Ebbesen, “Surface plasmon polaritons and their role in the enhanced transmission of light through periodic arrays of subwavelength holes in a metal film”, *Phys. Rev. Lett.* **92**, 107401 (2004).
9. R. Gordon, A. G. Brolo, A. McKinnon, A. Rajora, B. Leathem, and K. L. Kavanagh, “Strong polarization in the optical transmission through elliptical nanohole arrays”, *Phys. Rev. Lett.* **92**, 037401 (2004).
10. A. Degiron, H. J. Lezec, N. Yamamoto, and T. W. Ebbesen, “Optical transmission properties of a single sub-wavelength aperture in a real metal”, *Opt. Commun.* **239**, 61 – 66 (2004).
11. H. Lezec and T. Thio, “Diffracted evanescent wave model for enhanced and suppressed optical transmission through subwavelength hole arrays”, *Opt. Express* **12**, 3629 – 3651 (2004).

12. F. J. Garcia-Vidal, E. Moreno, J. A. Porto and L. Martin-Moreno, "Transmission of light through a single rectangular hole", *Phys. Rev. Lett.* **95**, 103901 (2005).
13. K. J. Webb and J. Li, "Analysis of transmission through small apertures in conducting films", *Phys. Rev. B* **73**, 033401 (2006).
14. A. Alu, F. Bilotti, N. Engheta, L. Vegni, "Metamaterial covers over a small aperture", *IEEE Trans. Antennas Propag.* **54**, 1632 – 1643 (2006).
15. J. Gomez-Rivas, C. Schotsch, P. H. Bolivar and H. Kurz, "Enhanced transmission of THz radiation through subwavelength holes", *Phys. Rev. B* **68**, 201306 (2003).
16. A. O. Cakmak, K. Aydin, E. Colak, Z. Li, F. Bilotti, L. Vegni, E. Ozbay, "Enhanced transmission through a subwavelength aperture using metamaterials", *Appl. Phys. Lett.* **95**, 052103 (2009).
17. K. Aydin, A. O. Cakmak, L. Sahin, Z. Li, F. Bilotti, L. Vegni, E. Ozbay, "Split-ring-resonator-coupled enhanced transmission through a single subwavelength aperture", *Phys. Rev. Lett.* **102**, 013904 (2009).
18. D. Ates, A. O. Cakmak, E. Colak, R. Zhao, C. M. Soukoulis, E. Ozbay, "Transmission enhancement through deep subwavelength apertures using connected split ring resonators", *Opt. Express* **18**, 3952–3966 (2010).
19. Z. Chen, A. Taflove, V. Backman, "Photonic nanojet enhancement of backscattering of light by nanoparticles: a potential novel visible-light ultramicroscopy technique", *Opt. Express* **12**, 1214–1220 (2004).
20. X. Li, Z. Chen, A. Taflove, V. Backman, "Optical analysis of nanoparticles via enhanced backscattering facilitated by 3-D photonic nanojets", *Opt. Express* **13**, 526–533 (2005).
21. Z. Chen, A. Taflove, X. Li, V. Backman, "Superenhanced backscattering of light by nanoparticles", *Opt. Lett.* **31**, 196–198 (2006).
22. A. Heifetz, S. Kong, A. V. Sahakian, A. Taflove, V. Backman, "Photonic Nanojets", *J. Comput. Theor. Nanosci.* **6**, 19791992 (2009).
23. M. K. Chin, D. Y. Chu, S-T. Ho, "Estimation of the spontaneous emission factor for microdisk lasers via the approximation of whispering gallery modes", *J. Appl. Phys.* **75**, 3302–3307 (1994).
24. J. L. Garcia-Pomar, M. Nieto-Vesperinas, "Waveguiding, collimation and subwavelength concentration in photonic crystals", *Opt. Express* **13**, 7997–8007 (2005).
25. F. J. Valdivia-Valero, M. Nieto-Vesperinas, "Resonance excitation and light concentration in sets of dielectric nanocylinders in front of a subwavelength aperture. Effects on extraordinary transmission", *Opt. Express* **18**, 6740-6754 (2010).
26. J. D. Jackson, *Classical Electrodynamics* (Wiley, New York, 1999).
27. J. A. Porto, F. J. Garcia-Vidal, J. B. Pendry, "Transmission resonances on metallic gratings with very narrow slits", *Phys. Rev. Lett.* **83**, 2845 – 2848 (1999).
28. N. Garcia, M. Nieto-Vesperinas, "Theory of electromagnetic wave transmission through metallic gratings of subwavelength slits", *J. Opt. A: Pure Appl. Opt. J. Opt. A: Pure Appl. Opt.* **9**, 490 - 495 (2007).
29. F. J. Valdivia-Valero, M. Nieto-Vesperinas, "Whispering gallery mode propagation in photonic crystals in front of subwavelength slit arrays. Interplay with extraordinary transmission", *Opt. Commun.* **284**, 1726 - 1733 (2011).
30. E. D. Palik, *Handbook of optical constants of solids* (Academic Press, New York, 1998).
31. J. Wenger, P. F. Lenne, E. Popov, H. Rigneault, J. Dintinger and T. Ebbesen, "Single molecule fluorescence in rectangular nano-apertures", *Opt. Express* **13**, 7035 – 7044 (2005).
32. H. Rigneault, J. Capoulade, J. Dintinger, J. Wenger, N. Bonod, E. Popov, T. W. Ebbesen and P. F. Lenne, "Enhancement of single-molecule fluorescence detection in subwavelength apertures", *Phys. Rev. Lett.* **95**, 117401 (2005).
33. J. Wenger, D. Gerard, J. Dintinger, O. Mahboub, N. Bonod, E. Popov, T. W. Ebbesen, H. Rigneault, "Emission and excitation contributions to enhanced single molecule fluorescence by gold nanometric apertures", *Opt. Express* **5**, 3008-3020 (2008).
34. B. D. Terris, H. J. Manin, D. Rugar, W. R. Studenmund and G. S. Kino, "Near - field optical data storage using a solid immersion lens", *Appl. Phys. Lett.* **85**, 25 – 27 (1994).
35. C. F. Bohren and D. R. Huffman, *Absorption and Scattering of Light by Small Particles* (Wiley, New York, 1998).

1. Introduction

Extraordinary transmission of light through apertures of size smaller than the wavelength λ has been a subject with a vast amount of interest [1, 2] since the first experiments [3] demonstrated that light could pass through subwavelength hole arrays of radius r , as well as through single apertures with a transmitted intensity much larger than as predicted by Bethe's theory [4]: $(r/\lambda)^4$. Many subsequent works [5, 6, 7, 8, 9, 10, 12, 13] deepened both theoretically [5] and experimentally [10, 11] in the understanding of this phenomenon for apertures practiced either in metallic or even in dielectric slabs; and proposals were made to even increase this transmission by a single aperture, for instance by introducing periodic corrugation on the slab

around a single hole [6], such that the beaming effect of the zero order of this grating could produce more directionally transmitted light through the hole. Other research to increase the efficiency of this process included employing other different aperture geometries [10, 12] or placing metamaterial slabs in front of the aperture [14]. Much work has been undertaken at optical frequencies, but there are also investigations at THz [15] as well as using the resonances of split ring resonators SRRs in the microwave regimes [16, 17]. In particular with the SRRs they experimentally showed [17] 740-fold transmission enhancement by amplifying the incoming wave into the subwavelength aperture with the help of the SRRs. Subsequent studies [18] even increased this transmittance amount.

The underlying concept for all these configurations is to produce a resonance that gives rise to intense and highly localized fields close to the aperture entrance, so that they couple with the resonance of the aperture, thus leading to enhanced fields at its exit and therefore to an enhanced transmission.

In this paper we study and illustrate this mechanism with numerical calculations capable of predicting or reproducing experimental results with great accuracy, but this time we shall employ as the resonant trigger a particle Mie resonance, in this case a *plasmonic nanoparticle* close to the subwavelength aperture entrance. Then the localized intense fields at the aperture will be due to those of the localized surface plasmon mode LSP_{mn} (where m and n stand for the eigenmode radial and angular numbers) of the particle which will subsequently couple and enhance the aperture mode TE_{uv} in its cavity, (where u and v stand for the mode numbers) and thus its transmittivity, hereafter referred to as an observed supertransmission peak. Plasmonic particles have not yet been employed for this task as far as we know.

In addition, since such a large intensity distribution, highly localized in the aperture, gives rise to an enhanced transmission, we inquire on the comparison of this plasmon morphology dependent resonance (MDR) coupling mechanism, which is resonant, to another one which is not; i. e. that of highly localized light focalization at the aperture by *excitation of a nanojet* [19, 20, 21, 22]. This last effect also gives rise to aperture transmittance enhancement, as we will show. Differences between those two effects as regards both the transmission peak and the transmittance spectrum shape, are discussed.

2. Numerical calculations

We shall employ a finite element method with FEMLAB of COMSOL (<http://www.comsol.com>) and will address a 2D configuration, since the essential features observed on coupling and resonance excitations are likewise obtained in 3D [19, 23]. Hence, we simulate the whole physical process through these numerical calculations. Details of the meshing geometry and convergence which leads to accurate results are given elsewhere [24, 25]. In the 2D geometry dealt with here, we have employed an incident wave, linearly p - polarized, namely with its magnetic vector \mathbf{H}_z perpendicular to the geometry of the XY - plane (i. e. the plane of the images shown in this work), and propagating in the Y - axis direction. In the case of plasmon excitation such a wave has a Gaussian profile at its focus: $\mathbf{H}_z(\mathbf{x}, \mathbf{y}) = |\mathbf{H}_{z0}| \exp(-x^2/2\sigma^2) \exp(i((2\pi/\lambda)y - \omega t))$, $|\mathbf{H}_{z0}|$ being the modulus amplitude, $2^{1/2}\sigma$ being the half width at half maximum (HWHM) of the beam, and λ its wavelength. In the case of nanojet excitation, a rectangular profile corresponding to a tapered time harmonic plane wave $\mathbf{H}_z(\mathbf{x}, \mathbf{y}) = |\mathbf{H}_{z0}| \exp(i((2\pi/\lambda)y - \omega t))$ has been employed. In both cases, wave profiles have been normalized to unity: $|\mathbf{H}_{z0}| = 1A/m$ (SI units), this corresponding to an incident energy flow magnitude $|\langle \mathbf{S}_0 \rangle| \approx 190W/m^2$ (SI units). In this way, both *plasmonic* and *nanojet* forming particles are cylinders with OZ axis (in fact, nanojets were first predicted in 2D for infinitely long cylinders [19] and later studied for other 3D particles [20, 21, 22]). For such a 2D geometry, it is well known that this choice of polarization (in contrast with s -

polarization) is the one under which the subwavelength slit presents homogeneous eigenmodes TE_{10} , i. e. which transmit and may lead to extraordinary transmission [25, 26, 27, 28, 29]. All refractive indices of the materials here considered are taken from [30] at the different addressed wavelengths.

3. Extraordinary transmission enhancement by localized plasmon excitation

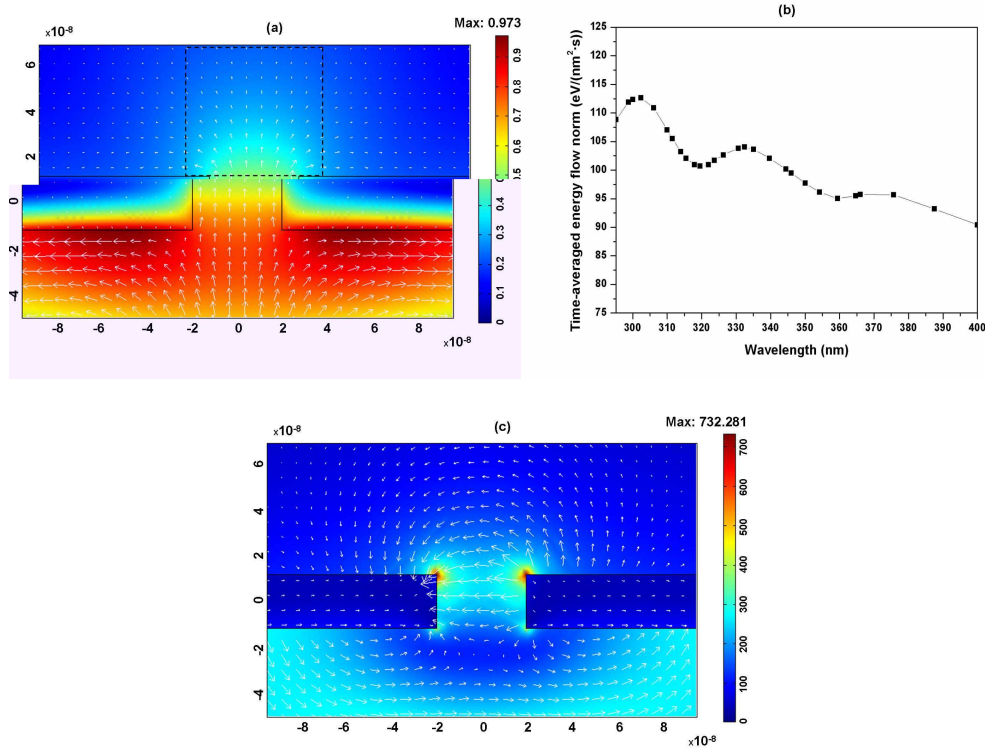


Fig. 1. (a) *Al* slab (refractive index $n_{Al} = 0.280 + i3.64$; slab width $D = 2.61 \mu\text{m}$; slab thickness $h = 23.76 \text{ nm}$; slit width $d = 39.59 \text{ nm}$) illuminated by a p - polarized Gaussian beam ($|\mathbf{H}_{z0}| = 1 \text{ A/m}$; spot size $2^{1/2}\sigma = 55.99 \text{ nm}$) at $\lambda = 302.4 \text{ nm}$ (i. e. exciting the TE_{10} slit mode). The light is incident upwards from below the slab. Magnetic field norm $|\mathbf{H}_z(\mathbf{r})|$ (in A/m (SI units)), in colors, and time - averaged energy flow $\langle \mathbf{S}(\mathbf{r}) \rangle$, in arrows (maximum arrow length = $998.41 \text{ eV}/(\text{nm}^2 \cdot \text{s})$). (b) Slab transmission evaluated as $|\langle \mathbf{S}(\mathbf{r}) \rangle|$, averaged over a square monitor area $A = ((3/2)d)^2 = 3526.58 \text{ nm}^2$ placed at the exit of the slit (see Fig. 1(a)). In this range of wavelengths, the highest transmission peak appears at $\lambda = 302.4 \text{ nm}$. (c) Detail of the electric near field $\mathbf{E}(\mathbf{r})$ (in V/m (SI units)) spatial distribution in both norm (colors) and vector (arrows) for the same configuration as in Fig. 1(a) at $\lambda = 302.4 \text{ nm}$.

Like in some other reported extraordinary transmission experiments [31, 32, 33], we consider a metallic *Al* slab of thickness $h = 23.76 \text{ nm}$ with a slit of width $d = 39.59 \text{ nm}$. As mentioned before, the *Al* refractive index at the wavelengths considered here are taken from Ref. [30], (it should be stressed that re-adapting the corresponding parameters of the configuration, one could equally employ other frequently used materials for the slab like, e.g. *Au*). We shall discuss this point in Section 5). The total width of the slab for the numerical calculation is $D = 2.61 \mu\text{m}$. This

slit alone is first illuminated with a Gaussian beam and the transmitted intensity is evaluated at the other side of the slab, close to the exit of the aperture, in a square of area $A = ((3/2)d)^2$, as shown in Fig. 1(a). In this range of wavelengths, at $\lambda = 302.4nm$ there is a maximum of the light energy transmitted by the slab into that square monitor, as shown by Fig. 1(b) for different wavelengths. Figure 1(a) also displays a picture, corresponding to this wavelength $\lambda = 302.4nm$ of peak transmission, of the spatial distribution of both $|\mathbf{H}_z(\mathbf{r})|$ and the energy flow given by the time - averaged Poynting vector $\langle \mathbf{S}(\mathbf{r}) \rangle$. Whereas Fig. 1(b) shows the magnitude $|\langle \mathbf{S}(\mathbf{r}) \rangle|$ transmitted into the aforementioned square area A at the aperture exit, at different λ . On the other hand, Fig. 1(c) illustrates the spatial distribution of the corresponding electric field near the slab and aperture. Surface waves, induced on scattering by the aperture edges, that propagate both along the slab and aperture surfaces are clearly seen in Fig. 1(a). Also charge concentrations, specially at the exit corners of the aperture, as a result of the excitation of the TE_{10} mode inside the aperture, are shown in Figs. 1(a) and 1(c). Specifically, Fig. 1(c) shows that as far as the electric field contribution is concerned, the induced currents in the aperture walls associated to the homogeneous TE_{10} mode produce strong charge concentrations at the vertices of the aperture exit. These two points of the 2D diagram behave as a dipole giving rise to a strong electric near field.

If now a plasmonic cylinder is placed in front of the entrance of the slit, i.e., at the side of the slab from which the beam is incident, the transmitted energy by this ensemble: slit plus particle, may increase dramatically.

To see this, and in order to argument it, let us first consider an isolated plasmonic cylinder with a Mie resonance at a wavelength not extremely far from that of the transmission peak of the aperture alone shown in Figs. 1(a) - 1(c). We shall address an Ag [30] cylinder of radius $r = 30nm$. The plasmon energy resonance peak of this cylinder alone, illuminated by the aforementioned Gaussian beam, occurs at $\lambda = 339.7nm$. This is illustrated by the spectrum of the mean Poynting vector magnitude near the cylinder in Fig. 2(a), which is evaluated at a narrow annulus around this particle surface as shown in Fig. 2(b), and exhibits in both Fig. 2(b) and Fig. 2(c) the characteristic strong dipolar electromagnetic field intensity distribution and large concentration of energy flow at this resonant wavelength. A comparison of the peaks in Fig. 2(a) and Fig. 1(b) already shows that the magnitude of the energy flow excited at the plasmon resonance in the Ag cylinder aforementioned surrounding annulus, is more than 100 times larger than that transmitted into the above mentioned exit square monitor by the aperture alone. Analogous conclusions by a factor 10 are derived for both the magnetic $|\mathbf{H}_z(\mathbf{r})|$ and electric $|\mathbf{E}(\mathbf{r})|$ field modulus which correspond to the isolated aperture and to the cylinder alone. Also, the excitation wavelengths corresponding to the peak transmission of the slit and of the cylinder plasmon are different [cf. Fig. 1(b) and Fig. 2(a)].

If we now place this cylinder close to the entrance of the slit as shown in Figs. 3(a) - 3(c), then the strong energy in this zone, due to the particle plasmon, will couple and transmit through the aperture via a feedback particle - slab/aperture, namely both aperture and particle modes will couple to each other creating a combined aperture - particle cavity mode at a red-shifted wavelength with respect to that of the particle alone. Notice that now, however, the effect of the particle is dominant upon the aperture transmission. Specifically, the presence of the slab slightly red-shifts the Mie resonance of the isolated cylinder to $\lambda = 344.4nm$, as expected, but the resulting enhancement of slit transmission at this new wavelength is now quite large. This is illustrated in Fig. 3(a) which shows an enhancement of transmitted energy almost five times larger than that around the particle alone, also with a much narrower bandwidth and hence with a larger quality factor, and more than 1000 times that of the transmittance of the slit alone (cf. Figs. 1(b) and 3(a)). The distributions of magnetic field and energy flow, as well as of electric field near the aperture are shown in Fig. 3(b) and Fig. 3(c) respectively, at this

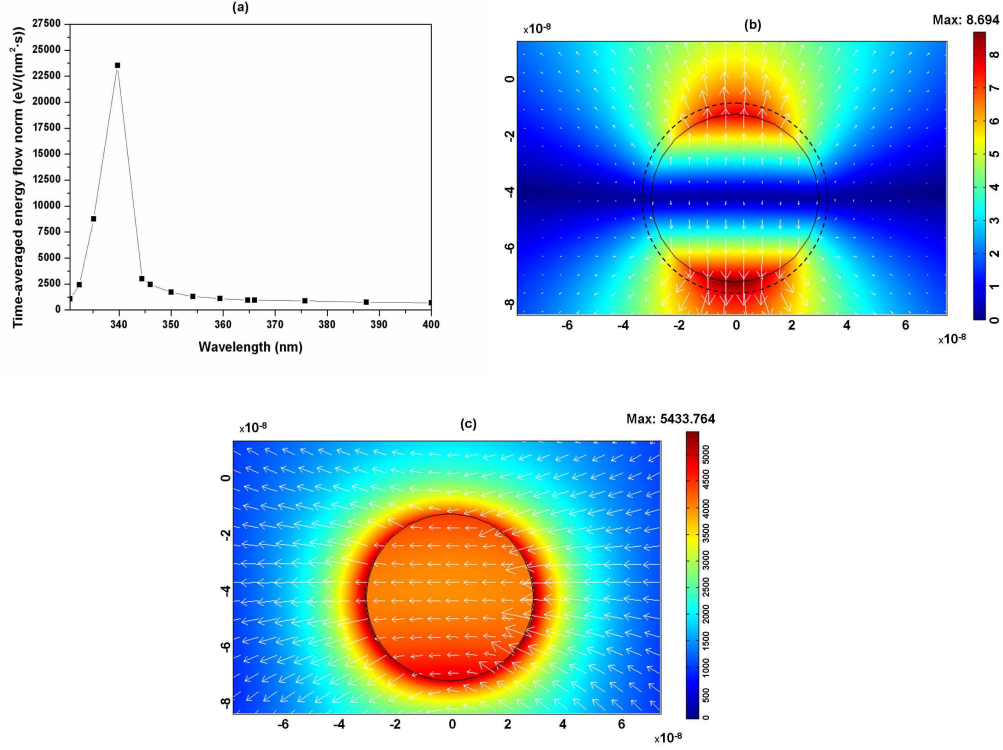


Fig. 2. (a) Response vs. wavelength of an isolated Ag cylinder (refractive index $n_{Ag} = 0.259 + i1.12$; radius $r = 30nm$) to a p - polarized Gaussian beam of the same σ as in incident from below with $|\mathbf{H}_{z0}| = 1A/m$ and $2^{1/2}\sigma = 59.99nm$, in time - averaged energy flow $|\langle \mathbf{S}(\mathbf{r}) \rangle|$, averaged in the area $A = \pi(33^2 - 30^2)nm^2 = 593.76nm^2$ of an annulus surrounding the particle (see the two concentric circles of Fig. 2(b)). The resonance peak occurs at $\lambda = 339.7nm$ (corresponding to the LSP_{21} cylinder mode). (b) Ag cylinder of Fig. 2(a), illuminated at $\lambda = 339.7nm$. Spatial distribution of magnetic field norm $|\mathbf{H}_z(\mathbf{r})|$ (in A/m (SI units)) in colors, and time - averaged energy flow $\langle \mathbf{S}(\mathbf{r}) \rangle$ in arrows (maximum arrow length = $59071.36eV/(nm^2 \cdot s)$). (c) Detail of the electric near field $\mathbf{E}(\mathbf{r})$ (in V/m (SI units)) distribution in both norm (colors) and vector (arrows) at $\lambda = 339.7nm$.

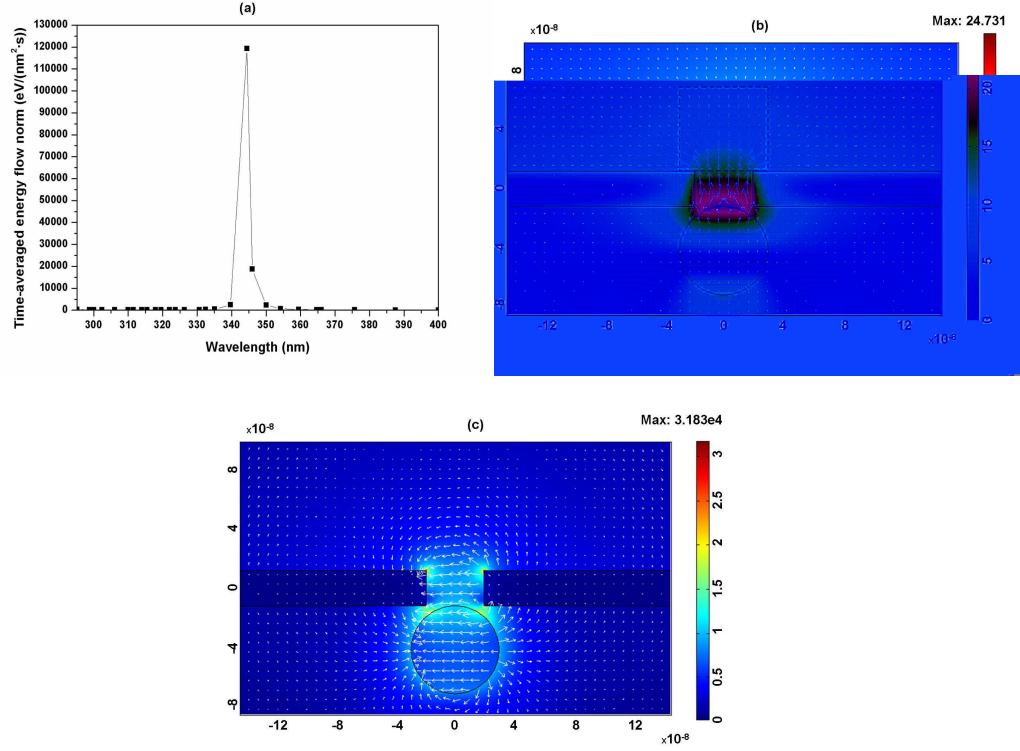


Fig. 3. (a) Transmission of the slit of Fig. 1(a) in presence of the plasmonic cylinder of Fig. 2(b), placed below the entrance of this slit as shown in Fig. 3(b). Time - averaged energy flow norm $|\langle \mathbf{S}(\mathbf{r}) \rangle|$, averaged over the area of the square monitor shown in Fig. 3(b), (which is the same as in Fig. 1(a) - 1(b)). The p - polarized light beam with the same σ as in Figs. 1, incides upwards from below the slab. The highest peak transmission appears at $\lambda = 344.4\text{nm}$ (corresponding to a red-shifted LSP_{21} cylinder resonance). (b) The Ag cylinder and aperture illuminated at $\lambda = 344.4\text{nm}$ (refractive index $n_{Al} = 0.364 + i4.17$; $n_{Ag} = 0.238 + i1.24$); showing the magnetic field norm $|\mathbf{H}_z(\mathbf{r})|$ (in A/m (SI units)) in colors, and time - averaged energy flow $\langle \mathbf{S}(\mathbf{r}) \rangle$ in arrows (maximum arrow length = $946829.51\text{eV}/(\text{nm}^2 \cdot \text{s})$). (c) Detail of the electric near field $\mathbf{E}(\mathbf{r})$ (in V/m (SI units)) distribution in both norm (colors) and vector (arrows) for the same configuration as in Fig. 3(b).

resonant wavelength of $\lambda = 344.4nm$. These showing large concentrations of field energy in the aperture and especially of charge and electric field at its exit corners, as well as partial penetration of the magnetic field through the Al boundaries of the slit. This is a phenomenon which usually occurs at thin apertures at the edges of the aperture. As a matter of fact, we stress here that *this enhancement of the aperture transmission due to the particle resonance occurs whether or not the aperture alone does supertransmit or not (of course, as long as the appropriate polarization, in this case p - waves, is chosen)*. If the aperture alone already produces extraordinary transmission, the presence of the resonant particle enhances it.

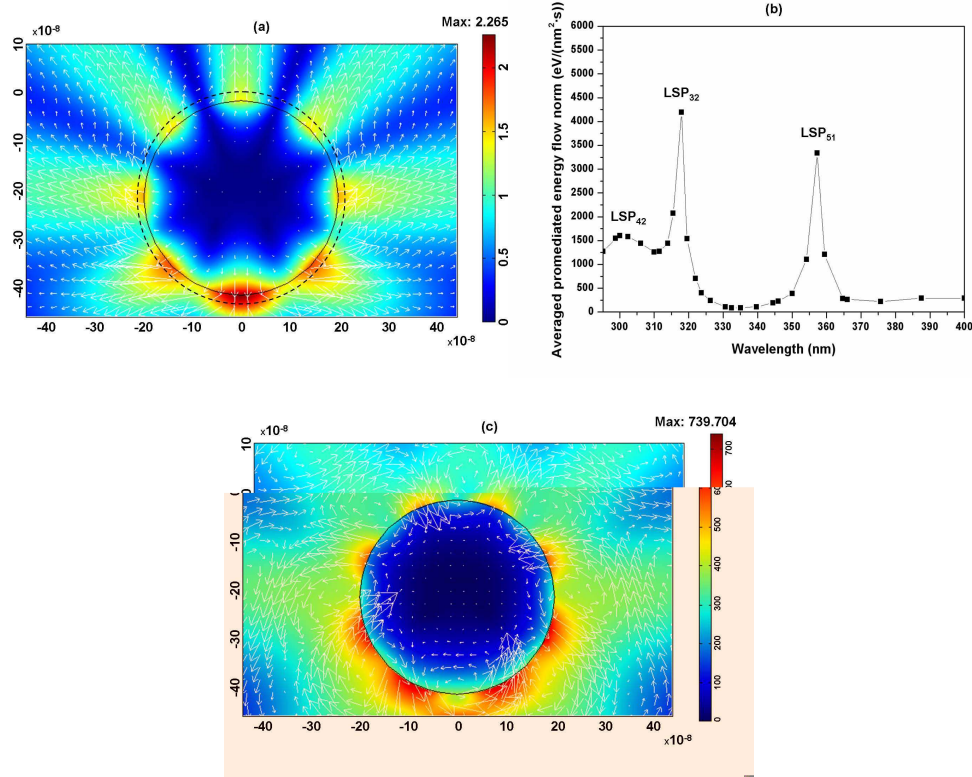


Fig. 4. (a) Ag cylinder (radius $r = 200nm$) illuminated by the same beam as in Figs. 3(a) - 3(c) at $\lambda = 300.0nm$ (refractive index $n_{Ag} = 1.513 + i0.955$; LSP_{42} cylinder resonance). Magnetic field norm $|\mathbf{H}_z(\mathbf{r})|$ (in A/m (SI units)) in colors, and time - averaged energy flow $\langle \mathbf{S}(\mathbf{r}) \rangle$ in arrows (maximum arrow length = $3067.37eV/(nm^2 \cdot s)$). (b) Cylinder response in time - averaged energy flow norm $|\langle \mathbf{S}(\mathbf{r}) \rangle|$, averaged over the area $A = \pi(220^2 - 200^2)nm^2 = 26389.38nm^2$ of an annulus surrounding the particle (see the two concentric circles in Fig. 4(a)) versus wavelength. The shown plasmon resonance peaks are: LSP_{42} , LSP_{32} and LSP_{51} located at $\lambda = 300.0nm$, $317.9nm$ and $357.3nm$ respectively. (c) Detail of the electric near field $\mathbf{E}(\mathbf{r})$ (in V/m (SI units)) distribution in both norm (colors) and vector (arrows) for the same situation as in Fig. 4(a).

Since transmission enhancement through the slit is linked to the induction of resonantly large field energies in its entrance that couple with the subwavelength slit mode, other larger plasmonic particles whose LSP modes produce such strong localized fields should also give rise to the same phenomenon. However, in this case the perturbation of the resonant wavelength introduced by the combination aperture - particle upon that of the particle alone should be more

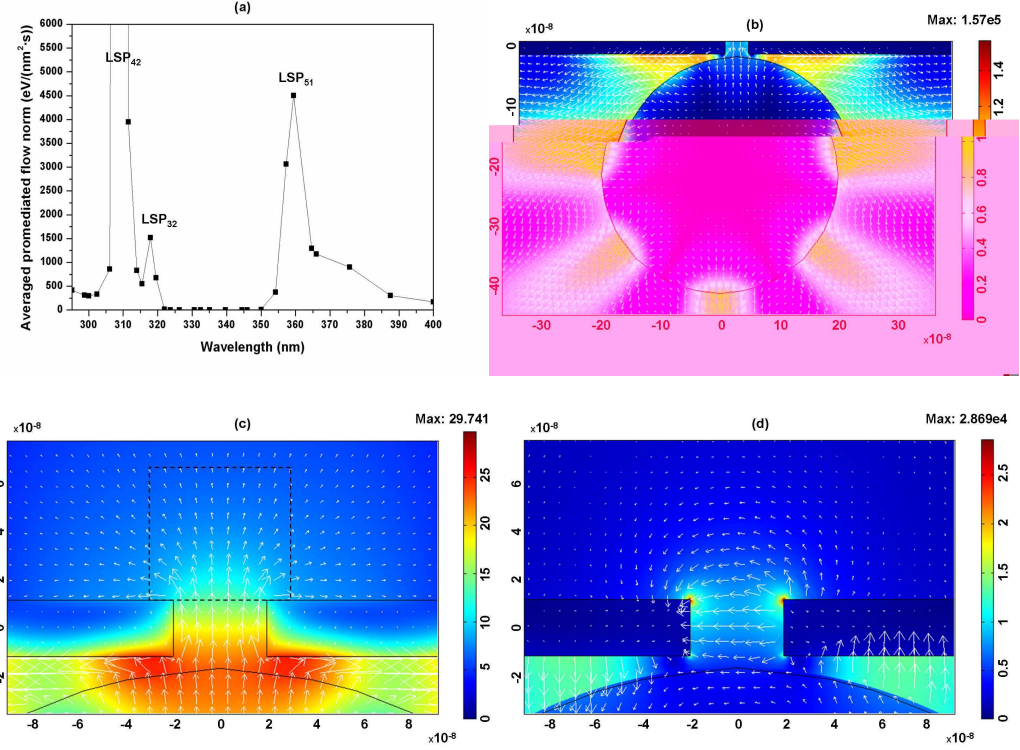


Fig. 5. (a) Response of the cylinder - slit/slab combination (i. e. those in Figs. 1(a) and 4(a)) in time - averaged energy flow norm $|\langle \mathbf{S}(\mathbf{r}) \rangle|$, averaged over the area of the same square monitor as in Figs. 1(a) - 1(b) and 3(a) - 3(b) (see the square of Fig. 5(c)). The shown resonance peaks are: LSP_{42} (it reaches the value of $\approx 120000 eV/(nm^2 \cdot s)$), LSP_{32} and LSP_{51} located at $\lambda = 310.0nm$, $317.9nm$ and $359.4nm$, respectively. The illumination beam has the same σ as in Figs. 1(a) - 1(c). (b) Magnetic near field norm $|\mathbf{H}_z(\mathbf{r})|$ (in A/m (SI units)) in colors, and averaged energy flow $\langle \mathbf{S}(\mathbf{r}) \rangle$ in arrows on illumination as in Fig. 5(a) at $\lambda = 310.0nm$ (refractive index $n_{Al} = 0.294 + i3.74$; $n_{Ag} = 1.323 + i0.647$; the LSP_{42} cylinder resonance is excited). This particle is placed at a distance of $5nm$ between its surface and the entrance plane of the Al slab. (c) Detail of Fig. 5(b). Magnetic field norm $|\mathbf{H}_z(\mathbf{r})|$ (in A/m (SI units)) in colors, and time - averaged energy flow $\langle \mathbf{S}(\mathbf{r}) \rangle$ in arrows (maximum arrow length = $979909.24 eV/(nm^2 \cdot s)$). (d) Detail of the electric near field $\mathbf{E}(\mathbf{r})$ (in V/m (SI units)) distribution in both norm (colors) and vector (arrows) for the same configuration as in Fig. 5(c).

noticeable. Let us study it. Figure 4(a) shows the spatial distribution of magnetic field magnitude and energy flow in the plasmon resonance LSP_{42} of an illuminated isolated Ag cylinder of radius $r = 200nm$ at $\lambda = 300.0nm$. As shown by the energy flow norm spectrum of this particle averaged near the particle surface in Fig. 4(b) (i. e. the annulus of Fig. 4(a)), this is not the plasmon excitation with the larger quality factor, which is the one at $\lambda = 317.9nm$ (corresponding to LSP_{32}). A detail of the distribution of electric field at $\lambda = 300.0nm$ is presented in Fig. 4(c). However, when this particle is placed close to the aperture entrance, the behavior of the system concerning slit transmission, beyond the redshift suffered by the cylinder modes, depends on the particular LSP mode excited on the particle surface. Two examples can be found in both the LSP_{32} and LSP_{51} modes, whose effect on enhancement in the slit transmission is lower and higher, respectively, than expected from their responses in energy concentration around the isolated cylinder surface (compare these resonant peaks in Fig. 4(b) for the cylinder alone with those of the transmitted energy in Fig. 5(a) when this particle is placed at the entrance of the slit). Nevertheless, the excitation of the red-shifted LSP_{42} on the cylinder below the slit does render, however, a huge transmission enhancement through the slit. Namely, at $\lambda = 310.0nm$, there is a dramatic change in the resonantly transmitted light by this combined system into the other side of the slit, as shown in Figs. 5(a) - 5(d). There the magnetic field, the electric field and the averaged energy flow transmitted at $\lambda = 310.0nm$ over the aforementioned square monitor placed at the exit of the slab, show a huge transmitted averaged energy flow, of large quality factor, which is comparable to that shown in Fig. 3(a) when the dipolar plasmonic cylinder was placed instead. Also, this LSP_{42} resonance wavelength in presence of this larger cylinder is quite separated from the larger energy resonance LSP_{32} of this cylinder alone, as seen on comparing Fig. 5(a) and Fig. 4(b). In addition, a comparison of Fig. 3(b) and Fig. 3(c) for the small cylinder placed below the aperture, with Figs. 5(b) - 5(d) that show the same quantities for this larger cylinder placed instead, evidences that such a large transmission enhancement is also produced by a large but rather delocalized energy distribution below the aperture, with local values in their spatial distribution, similar to the former. Hence, we conclude that from the point of view of concentrating most of the available excited energy in an effective way through transmission by producing high localized fields, it is better to employ small (even dipolar) plasmonic particles.

4. Comparison with extraordinary transmission by nanojet superfocusing

As concluded from the above calculations, enhancements and localization of the near field entering the subwavelength aperture at conditions such that the slit transmitting eigenmodes are excited, is behind the phenomenon of transmission enhancement. Then, one may inquire if any effect that gives rise to a large and highly localized field intensity distribution in the aperture, even if it is not resonant, will produce a similar phenomenon. To this end, we shall next consider a situation of superfocusing into the slit. This requires a large dielectric particle that acts as a near field lens, (see e. g. [34]). The geometrical parameters are now adapted to the spot size of the focused intensity produced by the particle. This superfocusing is done with a SiO_2 [30] cylinder of radius $1.9\mu m$, illuminated by a p-polarized rectangular-profile beam of width $w = 6\mu m$. A *nanojet* [19, 20, 21, 22] produced by superfocusing in the cylinder, of approximate half width at half maximum $HWHM = 120nm$, is produced at the opposite side of the surface of illumination in the cylinder, as illustrated for this particle alone in Fig. 6(a) for illumination at $\lambda = 400nm$, in which we have also drawn the slab with the slit to indicate the relative position between them and the cylinder when both objects are subsequently present. The enhancement and concentration of energy flow in the nanojet created on top of the cylinder is already evident in this figure. The slit that we next consider of width $d = 129.15nm$, is again in an Al slab, this time of thickness $h = 258.3nm$ and width $D = 6\mu m$. The energy flow transmitted by this

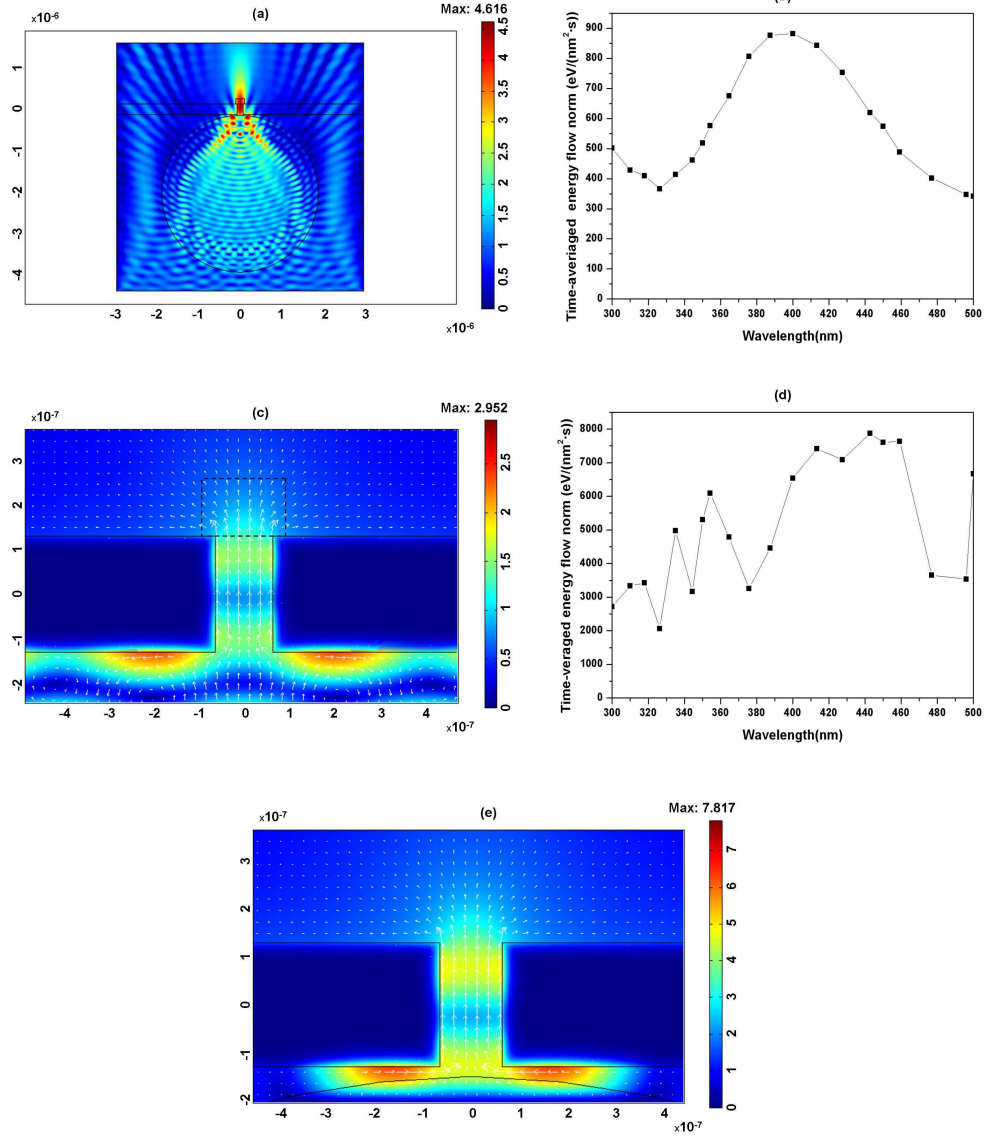


Fig. 6. (a) Spatial distribution of magnetic field norm $|\mathbf{H}_z(\mathbf{r})|$ (in A/m (SI units)) in colors. Time - averaged energy flow (amplitude $|\langle \mathbf{S} \rangle| = 19364.69 eV/(nm^2 \cdot s)$ for the hottest point of the nanojet whose width is $w \approx 120nm$) in an α -crystalline SiO_2 cylinder (refractive index $n_{silica} = 1.558$; cylinder radius $r = 1.9\mu m$) illuminated from below by a p-polarized unit amplitude rectangular beam (width $w = 6\mu m$) at $\lambda = 400.0nm$. The slab and slit to be used later have been drawn to see their relative positions in the following figures. (b) Transmission of an isolated metallic Al layer (width $D = 6\mu m$; thickness $h = 258.30nm$; slit width $d = 129.15nm$) in time - averaged energy flow norm $|\langle \mathbf{S}(\mathbf{r}) \rangle|$, averaged in the rectangular monitor of area $A = ((3/2)d)d = 25019.58nm^2$ at the exit of the aperture (see rectangle of Fig. 6(c)). A supertransmission peak arises at $\lambda = 400.0nm$ (corresponding to the slit TE_{10} mode). (c) Detail of the aperture whose response is studied in Fig. 6(b), illuminated at $\lambda = 400.0nm$ (refractive index $n_{Al} = 0.490 + i4.86$). Magnetic field norm $|\mathbf{H}_z(\mathbf{r})|$ (in A/m (SI units)) in colors, and $\langle \mathbf{S}(\mathbf{r}) \rangle$ in arrows (maximum arrow length = $4829.44 eV/(nm^2 \cdot s)$). (d) Response of the cylinder - slab combined system in time - averaged energy flow norm $|\langle \mathbf{S}(\mathbf{r}) \rangle|$, averaged in the same monitor as in Fig. 6(b). The system reaches its highest transmission at $\lambda = 442.8nm$. (e) Detail of transmission in the aperture evaluated as in Fig. 6(b) when the combined cylinder - slab system is illuminated as before at $\lambda = 442.8nm$ (refractive index $n_{Al} = 0.598 + i5.38$; $n_{silica} = 1.553$). Magnetic field norm $|\mathbf{H}_z(\mathbf{r})|$ (in A/m (SI units)) in colors, and $\langle \mathbf{S}(\mathbf{r}) \rangle$ in arrows (maximum arrow length = $43480.41 eV/(nm^2 \cdot s)$). The distance between the cylinder surface and the entrance plane of the Al slab is $20nm$.

slit alone in a rectangular monitor of area $((3/2)d)d = 25019.58nm^2$ is plotted in Fig. 6(b) as the incident wavelength λ of the aforementioned beam varies. As shown, there is a maximum of transmission of the slit at $\lambda = 400nm$. In Fig. 6(c) one sees the magnetic field magnitude and time-averaged energy flow spatial distribution $\langle \mathbf{S}(\mathbf{r}) \rangle$ near the slit corresponding to this illumination wavelength of maximum transmission by the slit alone.

If we now place the above cylinder in front of the slit, Fig. 6(d) shows versus λ the transmission of the energy flow into the above mentioned evaluation rectangular monitor. Also in this figure one sees that near the supertransmission wavelength, the shape of the transmission spectrum does not appreciably change except for ripples due to reflections in the cylinder - slit/slab cavity, even though its peak due to the presence of the nanojet increases by a factor of 8 and is red-shifted. As shown in the detail of Fig. 6(e), an enhancement of the aperture supertransmission is now obtained. This figure corresponds to the maximum of this quantity as plotted in Fig. 6(d), which occurs at $\lambda = 442.8nm$. Hence, again, the resonant transmittance of the aperture is red-shifted by the presence of the particle. Since the nanojet is not a resonance, but a subwavelength focusing effect, and the SiO_2 cylinder refractive index does not yield as much feedback with the aperture/slit via multiple reflections between them, the magnitude of this enhancement is much smaller, however, than that produced by the interaction between a particle plasmon resonance and the mode TE_{10} of the subwavelength slit, as shown in the previous examples with Ag particles.

5. Discussion and conclusions

In the above calculations, we have employed a region of wavelengths in the UV for observations of LSP excitation and in the violet for nanojets. As mentioned in the beginning of Section 3, one may equally choose other parameters and materials to observe similar phenomena. For instance, concerning the excitation of LSPs we have done other computations with different wavelengths, sizes and materials for the slab and the particle, obtaining similar qualitative results. For example, if one uses an Au particle of radius $a = 50nm$, this cylinder alone presents a LSP_{11} resonance peak at $\lambda = 496nm$ of time-averaged energy flow of about $476eV/(nm^2 \cdot s)$, with lower quality factor than that of Fig. 2(a), and whose line shape is rather similar to that of an Au sphere of radius $a = 20nm$, (this latter shown in Fig. 12.17 of [35]). Then by employing an Al slab with a slit whose parameters D , h and d are scaled with respect to those of Section 3 by a factor $5/3$, one obtains in the range of wavelengths around $\lambda = 496nm$ a tail of the transmitted energy for the slit alone, (with a value of about $133eV/(nm^2 \cdot s)$ near that wavelength), and a peak of transmission at $\lambda = 501nm$ of $450eV/(nm^2 \cdot s)$ for the combination slit-cylinder. This amount of transmitted energy is already similar to that around the cylinder alone, but it is more than 3 times larger than that of the slit alone. Analogous results are obtained concerning nanojet excitation with other materials and sizes.

Thus we conclude by stating the universality of the enhancement of transmission through a subwavelength aperture by excitation of particle LSP resonances, or in general by reinforcing and localizing the incident energy at the entrance of the aperture by other procedures like e.g via a nanojet or with other means of superfocusing. This enhancement is independent of whether or not the aperture alone produces extraordinary transmission, providing of course that the illumination is chosen such that a homogeneous (i. e. propagating) eigenmode is excited in its cavity; in particular, incident p-polarization is necessary when dealing with 2D slits. Transmission is dominated by either the LSP or by the creation of the nanojet. And it is more efficient the larger their lineshape Q factor is, depending on their sizes and hence on the resonant wavelength perturbation of the combined system slit - particle.

We hope that these results stimulate experiments in both 2D and 3D. In particular, if a plasmonic nanoparticle chain forms a signal and energy transporting waveguide, the aperture may

then constitute an interesting coupling device, to which high directionality of the transmitted light may be added if one, for instance, introduces periodic corrugation in the slab. A similar effect may occur for superfocused light and for nanoantennae in front of slits.

Acknowledgements

Work supported by the Spanish MEC through FIS2009-13430-C02-C01 and Consolider Nano-Light (CSD2007-00046) research grants, FJVV is supported by the last grant.